

# RSC Advances



This is an *Accepted Manuscript*, which has been through the Royal Society of Chemistry peer review process and has been accepted for publication.

*Accepted Manuscripts* are published online shortly after acceptance, before technical editing, formatting and proof reading. Using this free service, authors can make their results available to the community, in citable form, before we publish the edited article. This *Accepted Manuscript* will be replaced by the edited, formatted and paginated article as soon as this is available.

You can find more information about *Accepted Manuscripts* in the [Information for Authors](#).

Please note that technical editing may introduce minor changes to the text and/or graphics, which may alter content. The journal's standard [Terms & Conditions](#) and the [Ethical guidelines](#) still apply. In no event shall the Royal Society of Chemistry be held responsible for any errors or omissions in this *Accepted Manuscript* or any consequences arising from the use of any information it contains.

# A novel fabrication of nitrogen-containing carbon nanospheres with high rate capability as electrode materials for supercapacitors

Hui Peng<sup>a</sup>, Guofu Ma<sup>a\*</sup>, Kanjun Sun<sup>b</sup>, Jingjing Mu<sup>a</sup>, Xiaozhong Zhou<sup>a</sup>, Ziqiang Lei<sup>a\*</sup>

<sup>a</sup>Key Laboratory of Eco-Environment-Related Polymer Materials of Ministry of Education, Key Laboratory of Polymer Materials of Gansu Province, College of Chemistry and Chemical Engineering, Northwest Normal University, Lanzhou 730070, China.

<sup>b</sup>College of Chemistry and Environmental Science, Lanzhou City University, Lanzhou 730070, China.

## Abstract

Nitrogen-containing polyaniline-based carbon nanospheres (C-PANI) with diameter about 200 nm are prepared through a direct carbonization method using polyaniline (PANI) nanospheres as carbon precursor at different temperatures. The PANI nanospheres are synthesized via in-situ oxidation polymerization of aniline in the presence of sodium carboxymethyl cellulose as polymerization template. The C-PANI with 6.69% nitrogen content obtained at 800 °C (C-PANI-800) can achieve high capacitance of 359 F g<sup>-1</sup> at the current density of 1 A g<sup>-1</sup> in 6 M aqueous KOH electrolyte, meanwhile maintain excellent rate capability (81% retention at 20 A g<sup>-1</sup>). Furthermore, a symmetric supercapacitor fabricated with C-PANI-800 electrodes exhibits an energy density of 17.5 Wh kg<sup>-1</sup> at a power density of 227 W kg<sup>-1</sup> and superior cycle stability (only 4% loss after 5000 cycles), operated in the voltage range of 0-1.8 V in 0.5 mol L<sup>-1</sup> Na<sub>2</sub>SO<sub>4</sub> aqueous electrolyte.

---

\* Corresponding author. Tel./Fax: +86 931 7975121.

E-mail address: [magf@nwnu.edu.cn](mailto:magf@nwnu.edu.cn) (Guofu Ma); [leizq@nwnu.edu.cn](mailto:leizq@nwnu.edu.cn) (Ziqiang Lei)

## 1. Introduction

Supercapacitors have attracted considerable attention in recent years because of their high power density, subsecond charging, high rate capability, ultralong long cycle life and low maintenance cost [1-3]. According to their charge storage mechanisms, supercapacitors can be divided into electrochemical double-layer capacitors (EDLCs) and pseudocapacitors. The energy storage in EDLC is based on the adsorption of electrolyte ions on the electrically conductive porous electrodes, most commonly carbons. The other is pseudocapacitor, which has Faradic reactions at some metal oxides/hydroxides and conducting polymers [4]. Metal oxides such as  $\text{RuO}_2$ ,  $\text{MnO}_2$ ,  $\text{Ni}(\text{OH})_2$ ,  $\text{Co}_3\text{O}_4$ ,  $\text{BiVO}_4$  and so on [5-10], are widely recognized as the promising electrode materials due to their high specific capacitance. However, the expensive nature limits of  $\text{RuO}_2$  and poor electrical conductivity ( $10^{-5}$ - $10^{-6}$  S  $\text{cm}^{-1}$ ) of  $\text{MnO}_2$  [6], leading to limited in practical application. Conducting polymers have been found to have relatively poor cycling performance due to large volume change during repeated redox cycles processes which might lead to fatal degradation [11].

Among different types of supercapacitors, carbon materials are the most important and applicable electrode materials for commercial supercapacitors, attributing to their unique properties, such as large specific surface area, relatively low-cost, excellent electrical conductivity, extraordinary cycling stability in different solutions, and very friendly to the environment [12]. Various carbon materials, including activated carbon, mesoporous carbons, carbon nanotubes (CNTs), and graphene, have been investigated for use as electrode materials in EDLCs. However, the use of these individual carbon materials in high performance supercapacitors is limited by several factors, including the low specific capacitance of conventional activated carbon, the high cost of CNTs, and the unavoidable aggregation of graphene layers. Therefore, the majority of recent research on electrode materials has focused on the development of carbon materials with high specific capacitance and low cost [13]. Zhang research groups have reported that develop of graphene-coated hollow mesoporous carbon spheres and three-dimensional graphene-based hierarchically porous carbon composites by a flexible strategy for capacitive deionization [14-15].

Previous studies have revealed that besides of morphology and porosity structure, the capacitive

performance of the carbon materials is also determined by its surface functional groups, i.e. heteroatoms such as nitrogen, boron, sulphur and phosphorus in its structure [16-17]. Several efforts have been devoted to change the physicochemical properties of carbon materials by introducing heteroatoms, especially the nitrogen atom, due to the N-containing structures are believed to provide pseudocapacitance contributed from the redox faradaic reactions of these electrochemically active functional groups [18]. Several approaches, including chemical vapor deposition (CVD) in the presence of ammonia, the nitrogen plasma treatment, and the arc-discharge method have been exploited for the doping of nitrogen [19-21]. To the best of our knowledge, these methods suffer from some drawbacks, such as the requirement of toxic precursors, sophisticated equipment, special instruments and rigorous conditions. However, the carbonization of nitrogen-containing precursor is preferred because it is easier, more cost-effective, and more controllable for the N-doping content [17, 22-24]. Various nitrogen-containing precursors have been widely investigated to prepare nitrogen-doped porous carbons, including synthetic polymers [22], biomass [23] and ionic liquid [24]. Among which the most commonly used precursors are nitrogen-containing synthetic polymers, such as melamine resin and polyaniline are sustainable precursors for nitrogen-doped carbons [25-27].

Herein, we report a simple process to prepare nitrogen-containing carbon nanospheres using polyaniline (PANI) nanospheres as a carbon precursor. The PANI nanospheres are prepared by in-situ oxidation polymerization of aniline in the presence of sodium carboxymethyl cellulose as a polymerization template, and the nitrogen-containing carbon nanospheres were prepared by direct carbonized PANI nanospheres (C-PANI) at different temperatures. The C-PANI material shows high specific capacitance, outstanding rate capability, and excellent cycling stability, which are attributed to its high surface fraction of nitrogen and the high electrical conductivity, as well as to its well-balanced mesopore surface area and micropore surface area.

## 2. Experimental

### 2.1. Materials

Aniline (An, Shanghai Chemical Works, China) was distilled under reduced pressure. Sodium

carboxymethyl cellulose (CMC, Tianjin Yuanli Chemical Co., China), ammonium persulfate (APS, Tianjin Damao Chemical Co., China), and the other reagents were all analytical grade and were used as received without further treatment. All solutions were prepared in deionized water.

### 2.2. *Synthesis of PANI nanospheres.*

The PANI nanospheres were fabricated similar to our previous reported literature [21]. In a typical process, 0.10 g CMC was dissolved in 30 mL deionized water at room temperature. 0.40 g aniline monomer and 10 mL 1 M HCl solution were added to the above solution, and then the mixture was sonicated and stirred for 15 min. After cooling the mixture at 0-5 °C, 10 mL pre-cooled aqueous solution of APS (1.25 g) was added drop-by-drop into the above mixture. The reaction was carried out with magnetic stirring for 10 h in an ice bath. The resulting precipitate was collected by centrifugation and washed with deionized water and ethanol several times to remove APS and oligoaniline. Finally, the product was dried at 60 °C for 12 h to obtain a dark green powder.

### 2.3 *Carbonization of PANI nanospheres.*

The PANI nanospheres were carbonized in a horizontal furnace under pure nitrogen gas atmosphere. The typical process was performed as follows: a certain amount of PANI nanospheres were firstly heated to 450 °C with a heating rate of 5 °C min<sup>-1</sup>, and maintained for 2 h at this temperature. Then it was increased to the ultimate temperatures of 700, 800, 900 and 1000 °C, respectively, with a heating rate of 5 °C min<sup>-1</sup>, and keeping for 2 h to obtain the nitrogen-containing carbon nanospheres. The obtained samples were named as C-PANI-700, C-PANI-800, C-PANI-900 and C-PANI-1000, respectively.

### 2.4. *Characterizations*

The morphologies of pristine PANI and carbonized PANI at different temperatures were characterized by scanning electron microscopy (SEM, JSM-6701F, Japan) at an accelerating voltage of 5.0 kV, and transmission electron microscopy (TEM, JEM-1200EX, Japan). X-ray photoelectron spectroscopy (XPS) measurement was performed on an Escalab 210 system (Germany) using a monochromatic Al K $\alpha$  radiation source (ThermoVG Scientific). The products were analyzed by X-ray diffraction (XRD) on a diffractometer (D/Max-2400, Rigaku), in  $2\theta$  range from 5 to 80°, using Cu K $\alpha$  radiation ( $\lambda = 1.5418 \text{ \AA}$ ) at 40 kV, 100 mA. The elemental microanalysis (C, N and H) was carried out using the Elemental Analyzer Vario EL. The Brunauer-Emmett-Teller (BET) surface area ( $S_{\text{BET}}$ ) of the powders was analyzed by nitrogen adsorption in a Micromeritics ASAP 2020 nitrogen adsorption apparatus (U.S.A.).

### 2.5. Electrochemical measurements

A three-electrode system was first used to evaluate the electrochemical properties of the C-PANI in 6 mol L<sup>-1</sup> KOH aqueous solutions. The fabrication of the working electrodes as follow: 4 mg of the samples was ultrasonically dispersed in 0.4 mL of Nafion (0.25 wt %). The above suspension of 8  $\mu\text{L}$  was dropped onto the glassy carbon electrode using a pipet gun and dried at room temperature. Hg/HgO and carbon rod electrodes as reference and counter electrodes, respectively.

The symmetric two-electrode supercapacitors were assembled in 0.5 mol L<sup>-1</sup> Na<sub>2</sub>SO<sub>4</sub> aqueous solution using two electrodes with exactly the same mass into sandwich-type cells construction (electrode/separator/electrode). The working electrode was prepared by mixing the C-PANI-800, polyvinylidene fluoride (PVDF) and commercial carbon black (as conductive agent, purchased from Alfa Aesar) with a weight ratio of 80 : 10 : 10 in N-methyl-2-pyrrolidone (NMP)

to form a homogeneous slurry. The slurry was coated on nickel foam with a working area of 1.0 cm<sup>2</sup> and the electrodes were dried at 120 °C for 12 h and then weighted and pressed into sheets under 20 MPa. The positive and negative electrodes were pressed together and separated by a thin polypropylene film. The CV tests of symmetric cell were performed in the voltage range of 0-1.8 V.

Typical cyclic voltammetry (CV) curves and galvanostatic charge/discharge property of the samples were measured by using a CHI 660D (Chenghua, Shanghai China). Electrochemical impedance spectroscopy (EIS) measurements were performed with the Autolab PGSTAT 128N equipped (Eco-chemie, Netherland) with FRA module, the frequency ranging from 10 mHz to 100 kHz and an impedance amplitude of ±5 mV at open circuit potential. The measurement of cycle-life stability was performed with computer controlled cycling equipment (LAND CT2001A, Wuhan China).

### 3. Results and discussions

#### 3.1. Morphology and structure of C-PANI

The synthesis of PANI nanospheres were described in **Figure 1**. Firstly, the HCl solution added into the CMC solution promoted the dissociation of neutral -COONa into negatively charged -COO<sup>-</sup>. And then, the negatively charged CMC chains easily adsorbed -NH<sub>2</sub> groups of aniline monomer via an electrostatic interaction to form biopolymere monomer complexes. After the oxidant ammonium persulfate was introduced into the system, polyaniline was polymerized to form polyaniline nanospheres at low reaction temperature. Finally, Nitrogen-containing polyaniline-based carbon nanospheres were prepared with the direct carbonization method using

polyaniline nanospheres as a carbon precursor. In this work, nitrogen-containing polyaniline-based carbon nanospheres obtained at 800 °C, namely C-PANI-800, were characterized and used for supercapacitor applications unless otherwise specified.

Typical SEM images of pristine PANI and carbonized PANI at different temperatures are given in **Figure 2**. As seen in Figure 2a, as-prepared pristine PANI nanospheres have rough surface and many of these nanospheres aggregate together. Figure 2b-d show that C-PANI-700, C-PANI-800 and C-PANI-900 still retain PANI initial morphology after being carbonized, but surface morphology of carbonized PANI spheres become smoother than pristine PANI due to the high temperature carbonization. The average diameter of the carbon spheres is ca. 250 nm. Meanwhile, we can observe that these nanospheres have better uniform dispersion than those of the pristine PANI nanospheres. A more detailed structural study was carried out with high magnification SEM and TEM image (**Figure 3**). It is immediately apparent that the carbon spheres are relatively uniform, with an average size of ~250 nm.

The graphitization degrees of the carbonized PANI nanospheres can be determined by XRD and Raman spectroscopy analyses. The representative XRD patterns of the C-PANI from different carbonization temperature are presented in **Figure 4a**. Two broad diffraction peaks at around 24° and 43° are observed, ascribing to the (002) and (100) crystal planes of graphitic carbon, respectively, which suggests the low graphitization degree and the possible presence of amorphous carbon [28]. Figure 4b shows Raman spectra of the C-PANI-700, C-PANI-800 and C-PANI-900. There are two prominent peaks at 1600 cm<sup>-1</sup> (G-band) and 1340 cm<sup>-1</sup> (D-band) in spectra, corresponding to graphitic carbon phase with sp<sup>2</sup> electronic configuration, and defects and disorders structures in the graphene layers of carbon materials, respectively [29]. The intensity

ratio of the D peak to G peak ( $I_D/I_G$ ) is related to the amount of defects in the carbon materials.  $I_D/I_G$  values of e C-PANI-700, C-PANI-800 and C-PANI-900 are 0.97, 1.21 and 1.25, respectively, indicating that the C-PANI have a disorder structure and with the increase in the carbonization temperature more defects are generated in the C-PANI [30].

Figure 4c shows the  $N_2$  adsorption-desorption isotherms of carbonized PANI at different temperatures. Obviously, all the samples display  $N_2$  isotherms close to type IV with steep uptakes at low relative pressures and clear hysteresis loops, which indicated the coexistence of micropores and mesopores [31]. Moreover, a hysteresis loop at a higher pressure ( $P/P_0=0.90-0.99$ ) may be due to the macroporous adsorption among the gaps of carbon nanospheres. Based on the above analysis, the coexistence of micropores, mesopores and macropores can be confirmed. Figure 4d shows the pore size distribution of carbonized PANI at different temperatures. It is shown that the C-PANIs samples contain micropores (below 2 nm), small mesopores (peak pore at ca. 4.0), and large mesopores and macropores (from 10 to 100 nm). The results are consistent with  $N_2$  adsorption-desorption isotherms.

The BET surface area and pore structure characterization parameters of C-PANIs from different carbonization temperature are summarized in **Table 1**. It is found that the structural characters are seriously affected by the carbonization temperature. The C-PANIs samples show specific surface area ( $S_{BET}$ ) are in the range 359-607  $m^2 g^{-1}$  and total pore volume are in the range 0.31-0.47  $cm^3 g^{-1}$  during the carbonized temperature of 700-900  $^{\circ}C$ . In detail, the formation of micropores enhances the surface areas predominantly. However, the creation of mesoporous structures enlarges the pore volumes [32]. The contents of carbon, nitrogen and hydrogen of carbonized PANI at different temperatures are also listed in Table 1. As is seen in Table 1, the nitrogen

contents of the C-PANI-700, C-PANI-800 and C-PANI-900 are measured to be 9.44, 6.69, and 4.07 wt%, respectively, by elemental analysis. The result reveals that the nitrogen contents of samples decrease due to the increase of carbonization temperature. With increasing the temperature, the specific surface areas of C-PANI increase gradually owing to the volatilization of heteroatoms to form the micropores [26].

To understand the role of nitrogen functionalities in capacitive performance, it is necessary to clarify the types of nitrogen introduced onto the carbon surface via X-ray photoelectron spectroscopy (XPS) (**Figure 5**). As seen in Figure 5a, the peak at 284.1, 398.8, and 531.5 eV can be assigned to C1s, N1s, and O1s, respectively [21]. The C1s spectrum of C-PANI-800 (Figure 5b) has three distinct component peaks at binding energy of 284.7, 285.3 and 288.1 eV, representing graphitic carbon, carbonyl group and carboxyl group, respectively [33]. In addition, O1s spectrum of C-PANI-800 is shown in Figure 5c. The peak at the binding energy of 530.0 eV represents C=O. The peak at 532.1 eV is assigned to hydroxyl (C-OH) and ether (C-O-C) groups, while the peak at 533.0 eV corresponds to chemisorbed oxygen and/or water [34]. Figure 5d-f shows the N1s spectrum of C-PANI from different carbonization temperature, which can be fitted into four peaks at about 398.5, 400.5, 401.1 and 403.0 eV. These peaks are attributed to pyridinic nitrogen (N-6), pyrrolic nitrogen/pyridone nitrogen in association with oxygen functionality (N-5), quaternary nitrogen (N-Q), and pyridine-N-oxide (N-X), respectively [35]. Clearly, the content of pyridinic nitrogen (N-6) decreased with the increase of carbonization temperature. The C-PANI-800 was further characterized by element mapping images of carbon, oxygen and nitrogen to analyze the elemental distribution (**Figure 6**). The uniform distribution of yellow dots (N) suggests that nitrogen is homogeneously doped in the C-PANI. Some previous studies indicate that the carbons

have nitrogen-containing functional groups as well as oxygen functional groups can considerably contribute to an additional pseudo-capacitance. Specially, nitrogen located at the edges of graphite layers, that is, N-6 and N-5, are considered representing the pseudocapacitance effect. N-Q and N-X showed enhancing effects on the capacitance due to their positive charge and thus an improved electron transfer [36]. In addition, the carbons have heteroatom-containing functional groups as well as improve wettability, it can be providing a high electrode/electrolyte contact area and increasing chemically reactive sites [37].

### 3.2. Electrochemical properties of C-PANI

In order to evaluate the electrochemical properties of nitrogen doped PANI nanospheres as electrode material for supercapacitor, we first carried out cyclic voltammetry (CV) and galvanostatic charge-discharge tests in a three-electrode mode. **Figure 7a** gives the CV curves of C-PANI samples at a scan rate of  $10 \text{ mV s}^{-1}$  with the potential range of  $-1.0$  to  $0 \text{ V}$  in  $6 \text{ M KOH}$  aqueous electrolyte. The CV curves of all samples show near rectangular shapes with obvious hump peaks at lower potential, which is attributed to the pseudo-faradaic processes on the surface. In contrast, the CV curve of the C-PANI-800 exhibits larger area than that of others. Because of the linear relation between specific capacitance and CV curve area, it has a higher specific capacitance. It is found that the specific capacitance of C-PANI-700 decreases even the nitrogen content as high as  $9.44 \text{ wt\%}$ , this results should be mainly ascribed to the great decrease of the specific surface area. While the carbonization temperature is further increased to  $900 \text{ }^\circ\text{C}$ , the decrease in the area inside the curves implies a lowered capacitance, which could be attributed to the lowered functional groups [32]. **Figure 7b** presents CV curves for the C-PANI-800 electrode at various scan rates. When the scan rate increases to as high as  $200 \text{ mV s}^{-1}$ , the CV curve still

remains a rectangular-like shape with little polarization. This indicates that the C-PANI-800 electrode possesses a balanced specific surface area and N species, exhibiting excellent electrochemical behavior and good rate capability.

Galvanostatic charge/discharge curves of all carbonized samples at a current density of  $1 \text{ A g}^{-1}$  are shown in Figure 7c. The discharging time of the C-PANI-800 was significantly longer compared with that of other materials, indicating that the C-PANI-800 offers a much larger capacitor, which agrees well with those obtained from CV tests. Moreover, the curves are not perfect symmetric triangle feature, while a little deviation from the line can be observed. The deviation indicates that there is a small pseudo-capacitance besides the EDLC, which is attributed to the nitrogen attached to the carbon network [38]. The specific capacitance ( $C_m$ ) can be calculated according to the following equation:

$$C_m = C / m = (I \Delta t) / (\Delta V m) \quad (1)$$

where  $I$  is the current of discharge (A),  $\Delta t$  is the discharge time (S),  $\Delta V$  is the potential range during the discharge process, and  $m$  is the mass of active material within the electrode (g). The specific capacitance value of the C-PANI-800 is  $359 \text{ F g}^{-1}$  at current density of  $1 \text{ A g}^{-1}$ , which is much higher in comparison with the C-PANI-700, C-PANI-900, and C-PANI-1000. The sample C-PANI-800 of high specific capacitance may be attributed to the combined effect of a high nitrogen doping level changing the electron donor/acceptor characteristics of carbon and a large BET surface area increasing the surface area accessibility for electrolyte ion transport. The relationships between specific capacitance value and charge/discharge current density measured in a three-electrode system are presented in Figure 7d. A slight decrease in the specific capacitance of C-PANI-800 is observed as the current densities go from  $1$  to  $20 \text{ A g}^{-1}$ , indicating this electrode

material exhibits a good capacitance retention capability, for example, at 20 A g<sup>-1</sup> reaching 290 F g<sup>-1</sup>, which is ~81% of the value at 1 A g<sup>-1</sup>.

For practical application, the two-electrode symmetric supercapacitor was also fabricated to further investigate the electrochemical performance of the C-PANI-800 electrodes. Since the energy density ( $E$ ) is usually limited to the device capacitance ( $C$ ) and the operating voltage ( $V$ ) according to the equation  $E = 1/2CV^2$ . It is reported that the neutral Na<sub>2</sub>SO<sub>4</sub> aqueous electrolyte possesses a higher operation voltage than that of acid and alkali solutions [39]. Therefore, the C-PANI-800 symmetric supercapacitor was assembled with 0.5 M Na<sub>2</sub>SO aqueous solution electrolyte. The as-assembled symmetric cell was first measured at different potential windows at 20 mV s<sup>-1</sup>, and the resulted CV curves are exhibited in **Figure 8a**. The CV curves of the supercapacitor are rectangular-like shape even when the high voltage extends to 1.8 V, indicating ideal capacitive behavior and good reversibility. However, when the voltage increases to 2.0 V, the current is dramatically increased since the electrolyte is being decomposed with hydrogen and/or oxygen evolution. Therefore, the wide potential window of 1.8 V is chosen to further investigate the overall electrochemical performance of the symmetric cell.

The typical CV curves of the symmetric cell measured at different scan rates of 10~100 mV s<sup>-1</sup> between 0 and 1.8 V are displayed in Figure 8b. These CV curves still exhibit a nearly rectangular shape remains very well even at a high scan rate of 100 mV s<sup>-1</sup>, suggesting the symmetric cell possesses excellent rate capability and ideal electrochemical capacitive behavior with rapid diffusion of electrolyte ions to the interface of the electrode. Galvanostatic charge/discharge curves of the asymmetric cells were recorded with various current densities to further evaluate the electrochemical performance (Figure 8c). These typical triangular-shape charge/discharge curves

exhibit good symmetry at different current densities, which also demonstrating the ideal capacitive characteristic.

Figure 8d shows the Ragone plot related to energy and power densities of the C-PANI-800//C-PANI-800 symmetric cell in the potential range of 0-1.8 V. The specific energy density ( $E$ , Wh kg<sup>-1</sup>) and power density ( $P$ , W kg<sup>-1</sup>) for a supercapacitor cell were calculated from the discharge curves at different current densities using the following equations:

$$E=1/2CV^2 \quad (2)$$

$$P=E/t \quad (3)$$

where  $C$  is the specific capacitance of supercapacitor cell,  $V$  is voltage change during the discharge process after IR drop in V-t curve, and  $t$  is the discharge time. It is obviously that the symmetric cell exhibit the highest energy density is 17.5 Wh Kg<sup>-1</sup> at a power density of 227 W Kg<sup>-1</sup> and remained 8.3 Wh Kg<sup>-1</sup> at a power density of 2154 W Kg<sup>-1</sup>. The obtained maximum energy density is considerably higher than those previously reported symmetric carbon based supercapacitors, such as FHPC//FHPC (15.9 Wh Kg<sup>-1</sup>) [39], AC//AC (10 Wh Kg<sup>-1</sup>) [40], AC-based symmetric supercapacitors (16.9 Wh Kg<sup>-1</sup>) [41].

EIS analysis was used to gain a deep insight into the resistive and capacitive behavior of symmetric cell. **Figure 9a** shows Nyquist plot of symmetric cell with the small semicircle in the high-frequency region and the greater than 45° vertical curve in the low-frequency region, which results indicating a low charge-transfer resistance in the electrochemical system and a pronounced capacitive behavior with small diffusion resistance, respectively [42]. The impedance spectra were analyzed by the software of ZSimpWin on the basis of the electrical equivalent circuit (the inset of Figure 9a), where  $R_e$  stands for a combined resistance of ionic resistance of electrolyte, intrinsic

resistance of substrate and contact resistance at the active material/current collector interface. The diameter of the semicircle corresponds to the charge-transfer resistance ( $R_{ct}$ ) caused by Faradic reactions and electronic double layer capacitor ( $C_{dl}$ ) at the electrode/electrolyte interface. The slope of the  $45^\circ$  portion of the curve is called the Warburg resistance ( $Z_w$ ) and is a result of the frequency dependence of ion diffusion/transport in the electrolyte to the electrode surface;  $C_L$  is the limit capacitance [43]. The cycling stability measurement about 5000 cycles for symmetric cell was conducted using galvanostatic charge/discharge test at  $3 \text{ A g}^{-1}$  between 0 and 1.8 V (Figure 9b). It can be seen that the symmetric cell exhibits excellent cycling stability with 96% capacitance retention after 5000 cycles.

#### 4. Conclusions

In conclusion, the nitrogen-containing polyaniline-based carbon nanospheres (C-PANI) were successfully synthesized through direct carbonization strategy by using PANI nanospheres as a carbon precursor without any activation process. The C-PANI with 6.69% N content obtained at  $800^\circ\text{C}$  (C-PANI-800) can achieve a relatively high capacitance of  $359 \text{ F g}^{-1}$  at  $1 \text{ A g}^{-1}$  in 6 M KOH electrolyte, and even  $290 \text{ F g}^{-1}$  at a large current density of  $20 \text{ A g}^{-1}$ . Furthermore, the symmetric supercapacitor fabricated with C-PANI-800 electrodes delivers a high energy density of  $17.5 \text{ Wh kg}^{-1}$  at a power density of  $227 \text{ W kg}^{-1}$  operated in the voltage range of 0-1.8 V in  $0.5 \text{ mol L}^{-1}$   $\text{Na}_2\text{SO}_4$  aqueous electrolyte. In addition, a specific capacitance degradation of  $\sim 4\%$  over continuous 5000 cycles further demonstrated its good electrochemical stability as an electroactive material for supercapacitors application.

#### Acknowledgements

The research was financially supported by the Science and Technology Program of Gansu Province (NO.1308RJZA295, 1308RJZA265), the National Science Foundation of China (NO.21164009, 21174114), the program for Changjiang Scholars and Innovative Research Team in University (IRT1177), PhD Scientific Research starting Program of Lanzhou City University(LZCU-BS2013-11), Key Laboratory of Eco-Environment-Related Polymer Materials (Northwest Normal University) of Ministry of Education, and Key Laboratory of Polymer Materials of Gansu Province.

## References

- [1] P. Simon, Y. Gogotsi, *Nat Mater*, 2008, **7**, 845-854.
- [2] M. Inagaki, H. Konno, O. Tanaike, *J Power Sources*, 2010, **195**, 7880-7903.
- [3] H. Jiang, P. S. Lee, C. Li, *Energy Environ Sci*, 2013, **6**, 41-53.
- [4] G. P. Wang, L. Zhang, J. J. Zhang, *Chem Soc Rev*, 2012, **41**,797-828.
- [5] C. C. Hu, K. H. Chang, M. C. Lin, Y. T. Wu, *Nano Lett*, 2006, **6**, 2690-2695.
- [6] X. Lu, T. Zhai, X. Zhang, Y. Shen, L. Yuan, B. Hu, L. Gong, J. Chen, Y. Gao, J. Zhou, Y. Tong, Z. Wang, *Adv Mater*, 2012, **24**, 938-944.
- [7] H. Wang, H. S. Casalongue, Y. Liang, H. Dai, *J Am Chem Soc*, 2010, **132**, 7472-7477.
- [8] K. K. Lee, W. S. Chin, C. H. Sow, *J Mater Chem A*, 2014, **2**, 17212-17248.
- [9] Z. Khan, S. Bhattu, S. Haram, D. Khushalani, *RSC Adv*, 2014, **4**, 17378-17381.
- [10] X. Peng, L. Peng, C. Wu, Y. Xie, *Chem Soc Rev*, 2014, **43**, 3303-3323.
- [11] G. A. Snook, P. Kao, A. S. Best, *J Power Sources*, 2011, **196**,1-12.
- [12] Y. P. Zhai, Y. Q. Dou, D. Y. Zhao, P. F. Fulvio, R. T. Mayes, S. Dai, *Adv Mater*, 2011,

- 23,4828-4850.
- [13] L. Dai, D. W. Chang, J. B. Baek, W. Lu, *Small*, 2012, **8**, 1130-1166.
- [14] H. Wang, L. Shi, T. Yan, J. Zhang, Q. Zhong, D. Zhang, *J Mater Chem A*, 2014, **2**, 4739-4750.
- [15] X. Wen, D. Zhang, T. Yan, J. Zhang, L Shi, *J Mater Chem A*, 2013, **1**, 12334-12344.
- [16] Z. H. Wen, X. C. Wang, S. Mao, Z. Bo, H. Kim, S. M. Cui, G. H. Lu, X. L. Feng, J. H. Chen, *Adv Mater*, 2012, **24**, 5610-5616.
- [17] J. P. Paraknowitsch, A. Thomas, *Energy Environ Sci*, 2013, **6**, 2839-2855.
- [18] G. Lota, K. Lota, E. Frackowiak, *Electrochem Commun*, 2007, **9**, 1828-1832.
- [19] Y. Z. Xue, B. Wu, L. Jiang, Y. L. Guo, L. P. Huang, J. Y. Chen, J. H. Tan, D. C. Geng, B. R. Luo, W. P. Hu, G. Yu, Y. Q. Liu, *J Am. Chem Soc*, 2012, **134**, 11060-11063.
- [20] Y. Y. Shao, S. Zhang, M. H. Engelhard, G. S. Li, G. C. Shao, Y. Wang, J. Liu, I. A. Aksay, Y. H. Lin, *J Mater Chem*, 2010, **20**, 7491-7496.
- [21] N. Li, Z. Y. Wang, K. K. Zhao, Z. J. Shi, Z. N. Gu, S. K. Xu, *Carbon*, 2010, **48**, 255-259.
- [22] M. Vujković, N. Gavrilov, I. Pašti, J. Krstić, J. Travas-Sejdic, G. Ćirić-Marjanović, S. Mentus, *Carbon*, 2013, **64**, 472-486.
- [23] Z. Li, L. Zhang, B. S. Amirkhiz, X. H. Tan, Z. W. Xu, H. L. Wang, B. C. Olsen, C. M. B. Holt, D. Mitlin, *Adv Energy Mater*, 2012, **2**, 431-437.
- [24] J. P. Paraknowitsch, J. Zhang, D. Su, A. Thomas, M. Antonietti, *Adv Mater*, 2010, **22**, 87-92.
- [25] D. Hulicova, J. Yamashita, Y. Soneda, H. Hatori, M. Kodama, *Chem Mater*, 2005, **17**, 1241-1247.
- [26] D. S. Yuan, T. X. Zhou, S. L. Zhou, W. J. Zou, S. S. Mo, N. N. Xia, *Electrochem Commun*,

- 2011, **13**,242-246.
- [27] H. Peng, G. F. Ma, W. M. Ying, A. D. Wang, H. H. Huang, Z. Q. Lei, *J Power Sources*, 2012, **211**, 40-45.
- [28] Y. Z. Jin, C. Gao, W. K. Hsu, Y. Q. Zhu, A. Huczko, M. Bystrzejewski, M. Roe, C. Y. Lee, S. Acquah, H. Kroto, D. R. M. Walton, *Carbon*, 2005, **43**, 1944-1953.
- [29] M. S. Dresselhaus, A. Jorio, M. Hofmann, G. Dresselhaus, R. Saito, *Nano Lett*, 2010, **10**, 751-758.
- [30] M. A. Pimenta, G. Dresselhaus, M. S. Dresselhaus, L. G. Cançado, A. Jorio, R. Saito, *Phys Chem Chem Phys*, 2007, **9**, 1276-1290.
- [31] Y. Fang, D. Gu, Y. Zou, Z. X. Wu, F. Y. Li, R. C. Che, Y. H. Deng, B. Tu, D. Y. Zhao, *Angew Chem Int. Ed*, 2010, **49**, 7987-7991.
- [32] H. Zhu, X. Wang, X. Liu, X. Yang, *Adv Mater*, 2012, **24**, 6524-6529.
- [33] N. Xiao, D. Lau, W. H. Shi, J. X. Zhu, X. C. Dong, H. H. Hng, Q. Y. Yan, *Carbon*, 2013, **57**, 184-190.
- [34] B. Xu, D. Zheng, M. Jia, G. Cao, Y. Yang, *Electrochim Acta*, 2013, **98**,176-182.
- [35] Z. W. He, Q. F. Lü, Q. Lin, *Bioresource technol*, 2013, **127**, 66-71.
- [36] D. Hulicova-Jurcakova, M. Seredych, G. Q. Lu, T. J. Bandosz, *Adv Funct Mater*, 2009, **19**, 438-447.
- [37] Y. Huang, J. J. Liang, Y. S. Chen, *Small*, 2012, **8**, 1805-1834.
- [38] W. R. Li, D. H. Chen, Z. Li, Y. F. Shi, Y. Wan, J. J. Huang, J. J. Yang, D. Y. Zhao, Z. Y. Jia, *Electrochem Commun*, 2007, **9**, 569-573.
- [39] Q. Wang, J. Yan, Y. B. Wang, T. Wei, M. L. Zhang, X. Y. Jing, Z. J. Fan, *Carbon*, 2014, **67**,

- 119-127.
- [40] L. Demarconnay, E. Raymundo-Piñero, F. Béguin, *Electrochem Commun*, 2010, **12**, 1275-1278.
- [41] X. Z. Sun, X. Zhang, H. T. Zhang, D. C. Zhang, Y. W. Ma, *J Solid State Electrochem*, 2012, **16**, 2597-2603.
- [42] J. G. Wang, Y. Yang, Z. H. Huang, F. Y. Kang, *Carbon*, 2013, **61**, 190-199.
- [43] J. Chang, M. Jin, F. Yao, T. H. Kim, V. T. Le, H. Yue, F. Gunes, B. Li, A. Ghosh, S. Xie and Y. H. Lee, *Adv Funct Mater*, 2013, **23**, 5074-5083.

**Figure captions**

**Figure 1.** Schematic of the preparation process of nitrogen-containing polyaniline-based carbon nanospheres

**Figure 2.** SEM images of (a) pristine PANI, (b) C-PANI-700, (c) C-PANI-800 and (d) C-PANI-900.

**Figure 3.** (a) High magnification SEM image and (b) TEM image of the C-PANI-800.

**Figure 4.** (a) XRD pattern and (b) Raman spectra of C-PANI at different temperatures; (c) Nitrogen adsorption-desorption isotherms and (d) pore size distribution curves of C-PANI at different temperatures.

**Table 1.** Elemental analysis, BET surface area and pore structure characterization parameters of C-PANI from different carbonization temperature.

**Figure 5.** XPS spectra of the C-PANI materials: (a) survey spectrum, (b) C 1s spectrum of C-PANI-800, (c) O 1s spectrum of C-PANI-800 and (d-f) N 1s spectrum of C-PANI.

**Figure 6.** The element mapping images of C-PANI-800 sample.

**Figure 7.** (a) Cyclic voltammograms of C-PANI electrodes at a scan rate of  $10 \text{ mV s}^{-1}$  in 6 M KOH solution; (b) Cyclic voltammograms of C-PANI-800 electrode at different scan rates. (c) Galvanostatic charge/discharge curves of C-PANI electrodes at a current density of  $1 \text{ A g}^{-1}$ ; (d) Discharge capacitances of C-PANI electrodes at various current densities.

**Figure 8.** (a) CV curves of the symmetric two-electrode cell at different voltage windows in 0.5 M  $\text{Na}_2\text{SO}_4$  aqueous electrolytes; (b) CV plots of the C-PANI-800 electrode at various scan rates; (c) Galvanostatic charge/discharge curves of C-PANI-800 electrodes at various current densities; (d) Ragone plot related to energy and power densities of the C-PANI-800 electrode.

**Figure 9.** (a) Nyquist plots of two-electrode symmetric cell base on C-PANI-800 electrodes (the inset of modeled equivalent circuit); (b) Cycling stability of the symmetric cell.

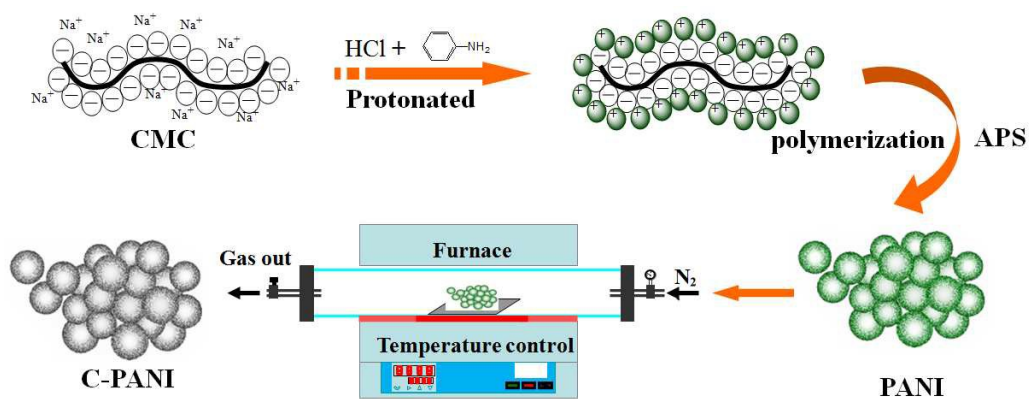


**Figure 1.** Schematic of the preparation process of nitrogen-containing polyaniline-based carbon nanospheres.

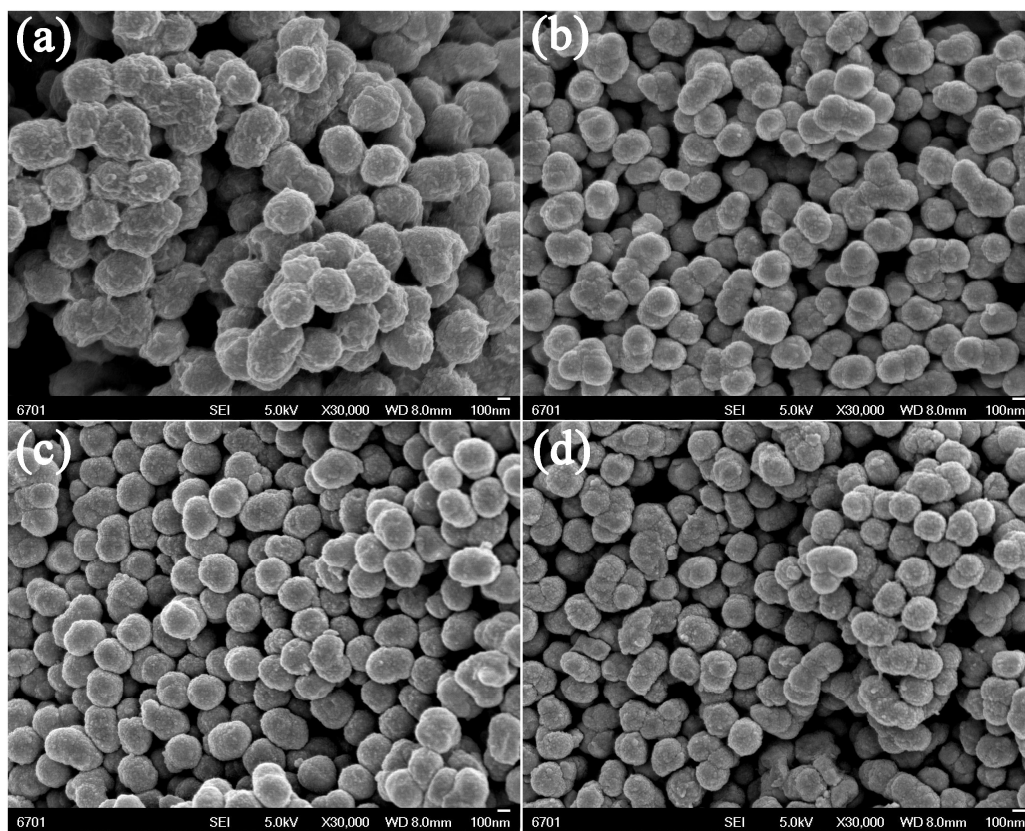


**Figure 2.** SEM images of (a) pristine PANI, (b) C-PANI-700, (c) C-PANI-800 and (d) C-PANI-900.

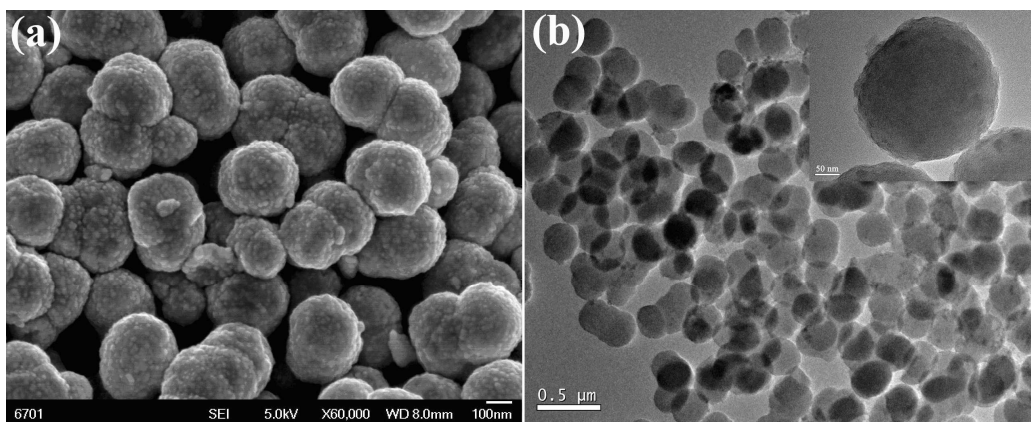


**Figure 3.** (a) High magnification SEM image and (b) TEM image of the C-PANI-800.

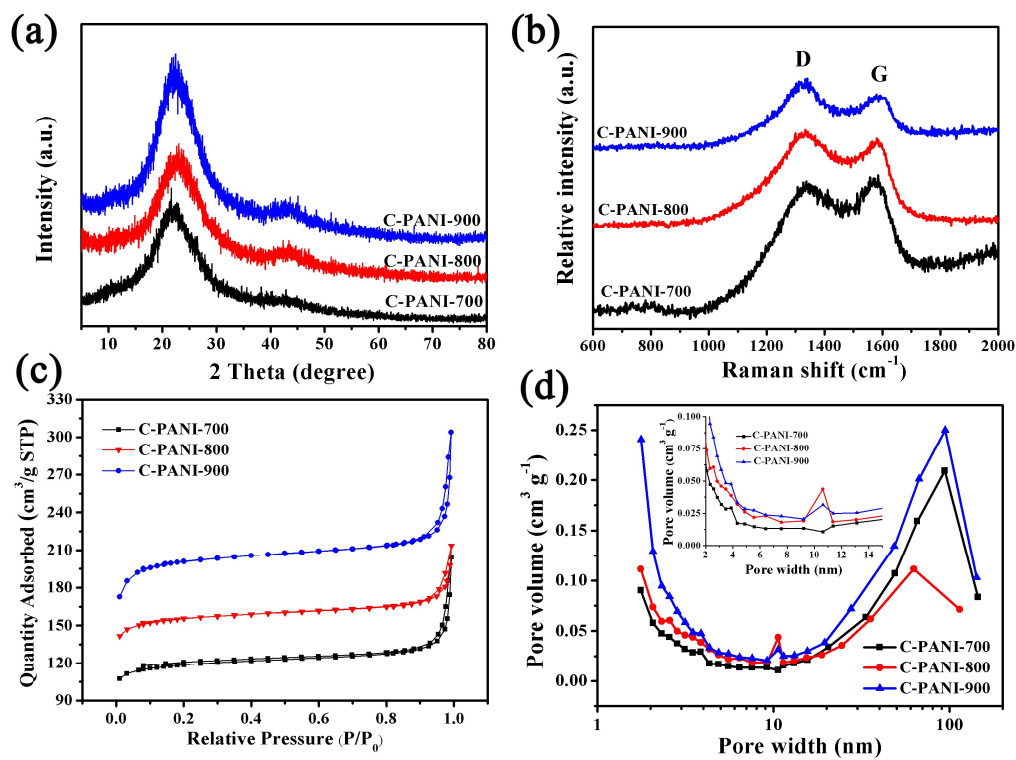


**Figure 4.** (a) XRD pattern and (b) Raman spectra of C-PANI at different temperatures; (c) Nitrogen adsorption-desorption isotherms and (d) pore size distribution curves of C-PANI at different temperatures.

**Table 1.** Elemental analysis, BET surface area and pore structure characterization parameters of C-PANI from different carbonization temperature.

Samples	Elemental analysis			$S_{\text{BET}}^{\text{a}}$	$S_{\text{mic}}^{\text{b}}$	$D^{\text{c}}$	$V_{\text{total}}^{\text{d}}$	$V_{\text{micro}}^{\text{e}}$
	C %	N %	H %	( $\text{m}^2 \text{g}^{-1}$ )	( $\text{m}^2 \text{g}^{-1}$ )	(nm)	( $\text{cm}^3 \text{g}^{-1}$ )	( $\text{cm}^3 \text{g}^{-1}$ )
C-PANI-700	76.90	9.44	1.86	359	298	3.52	0.31	0.16
C-PANI-800	76.04	6.69	1.71	422	345	3.02	0.32	0.18
C-PANI-900	73.23	4.07	2.08	607	403	3.09	0.47	0.26

a) Specific surface area determined according to BET (Brunauer-Emmett-Teller) method. b) Micropore surface area from t-plot method. c) Adsorption average pore diameter. d) Total pore volume. e) Volume of micropores.

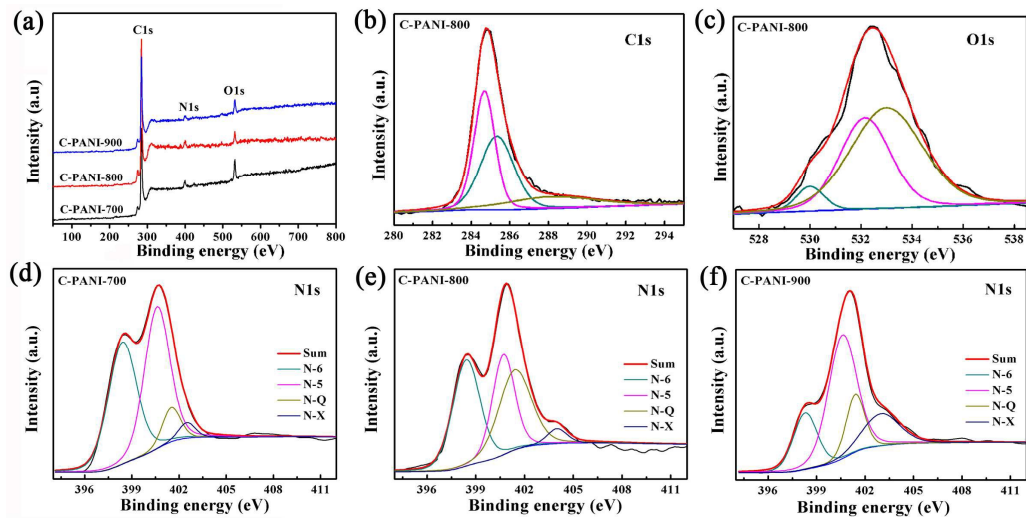


**Figure 5.** XPS spectra of the C-PANI materials: (a) survey spectrum, (b) C 1s spectrum of C-PANI-800, (c) O 1s spectrum of C-PANI-800 and (d-f) N 1s spectrum of C-PANI.

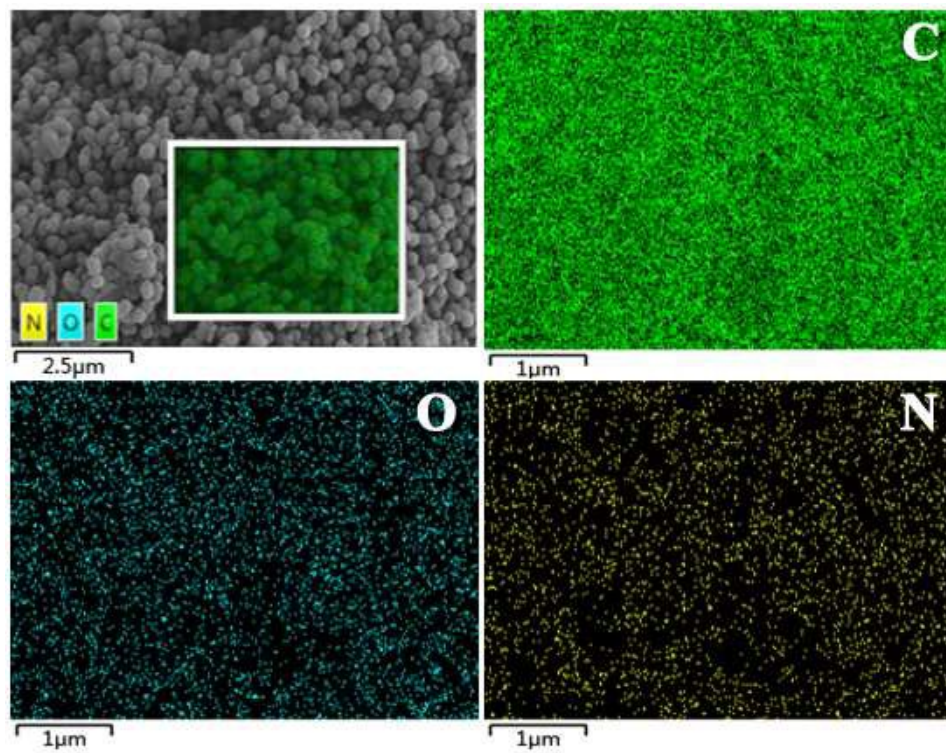


**Figure 6.** The element mapping images of C-PANI-800 sample.

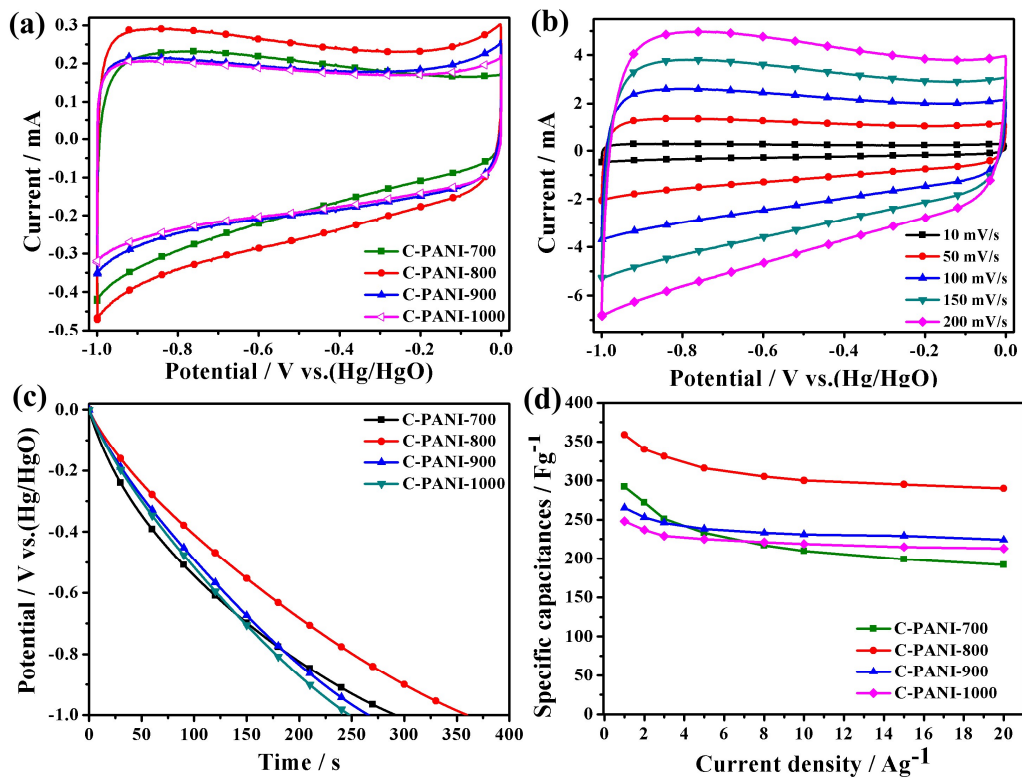


**Figure 7.** (a) Cyclic voltammograms of C-PANI electrodes at a scan rate of 10 mV s<sup>-1</sup> in 6 M KOH solution; (b) cyclic voltammograms of C-PANI-800 electrode at different scan rates. (c) Galvanostatic charge/discharge curves of C-PANI electrodes at a current density of 1 A g<sup>-1</sup>; (d) Discharge capacitances of C-PANI electrodes at various current densities.

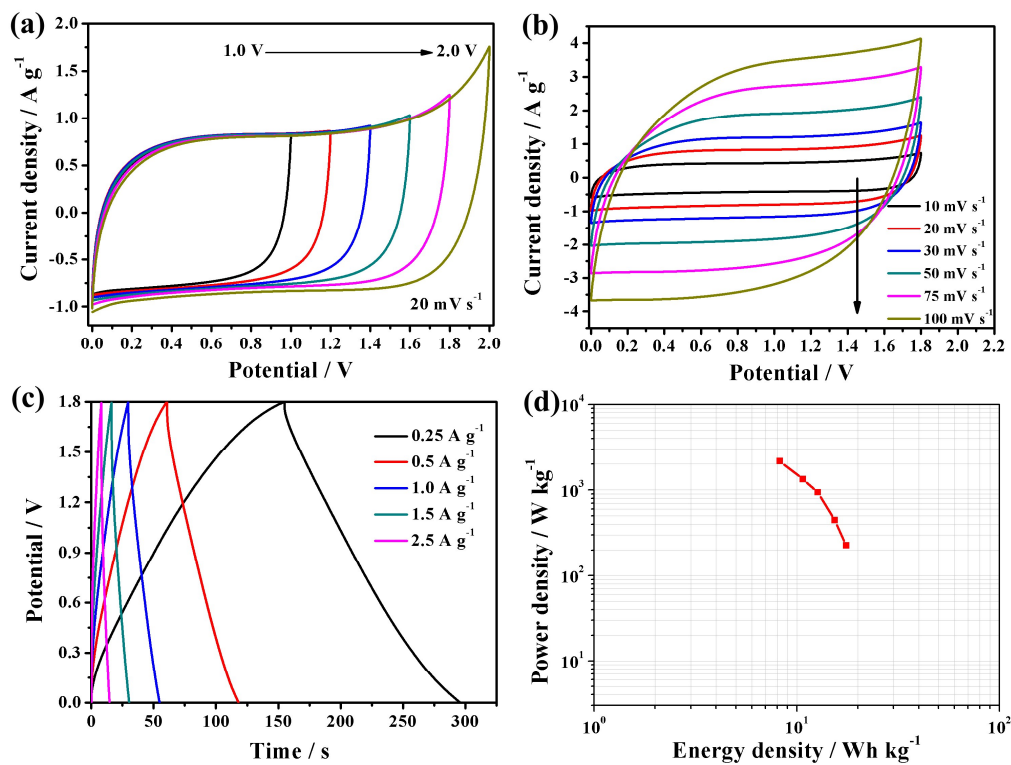


**Figure 8.** (a) CV curves of the symmetric two-electrode cell at different voltage windows in 0.5 M Na<sub>2</sub>SO<sub>4</sub> aqueous electrolytes; (b) CV plots of the C-PANI-800 electrode at various scan rates; (c) Galvanostatic charge/discharge curves of C-PANI-800 electrodes at various current densities; (d) Ragone plot related to energy and power densities of the C-PANI-800 electrode.

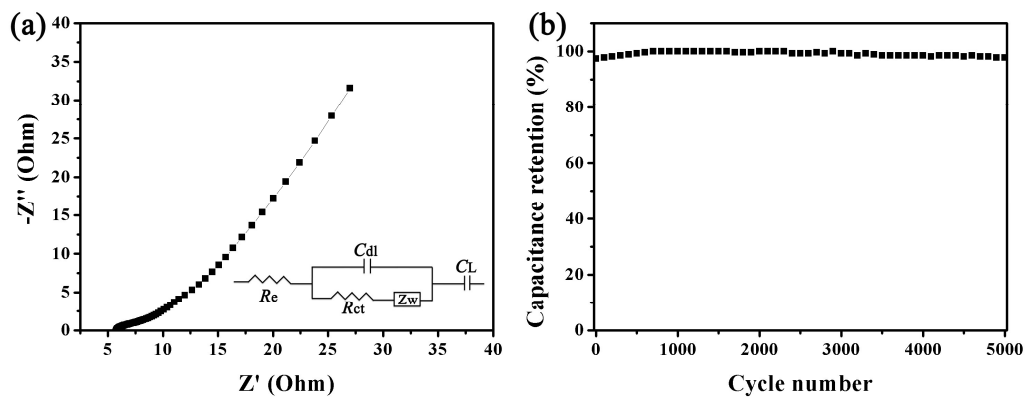


**Figure 9.** (a) Nyquist plots of two-electrode symmetric cell base on C-PANI-800 electrodes (the inset of modeled equivalent circuit); (b) Cycling stability of the symmetric cell.